Remote Sensing of Environment 113 (2009) 1331–1342

Contents lists available at ScienceDirect

Remote Sensing of Environment

journal homepage: www.elsevier.com/locate/rse

A multi-sensor comparison of sulphur dioxide emissions from the 2005 eruption of Sierra Negra volcano, Galápagos Islands

H.E. Thomas [a,b,*], I.M. Watson [a,b], C. Kearney [a], S.A. Carn [b], S.J. Murray [a]

[a] Department of Earth Sciences, University of Bristol, Wills Memorial Building, Queen's Road, Bristol, BS8 1RJ, UK
[b] Department of Geological and Mining Engineering and Sciences, 630 Dow Environmental Science and Engineering Building, 1400 Townsend Drive, Houghton, Michigan 49931-1295, USA

ARTICLE INFO

Article history:
Received 19 December 2008
Received in revised form 26 February 2009
Accepted 28 February 2009

Keywords:
MODIS
OMI
TOMS
Sulphur dioxide
Sensor comparison
Satellite remote sensing

ABSTRACT

Sulphur dioxide retrievals of three satellite-based sensors (the Total Ozone Mapping Spectrometer, the Ozone Monitoring Instrument and the Moderate Resolution Imaging Spectroradiometer) were performed on the volcanic cloud from the Sierra Negra, Galápagos Islands eruption of October 22 to October 30, 2005. Near-coincidental plume acquisitions on 23 October from each of the sensors were compared spatially on a pixel-by-pixel basis in order to assess the level of agreement between the retrievals. The variation in pixel size and shape between sensors was accounted for by resampling MODIS data to the geometry of the UV sensors.

It was found that correlations between retrievals were wide ranging with estimates of total tonnage ranging from 60 kt up to 1800 kt. Spatial comparisons show variation according to plume altitude and overpass time and are compounded by interference from other volcanic species as well as individual instrument error.

The comparison of these sensors provides an insight into the relative merits of each method and illustrates the usefulness of a holistic approach to satellite remote sensing of sulphur dioxide. This will permit the development of more robust retrieval schemes and therefore increasingly reliable estimations of volcanic SO_2 emissions.

© 2009 Elsevier Inc. All rights reserved.

1. Introduction

Sulphur dioxide (SO_2) is one of the most commonly measured volcanic gas species. It is a useful indicator of pre-eruptive activity (Caltabiano et al., 1994; Edmonds et al., 2003; Sutton et al., 2001), whilst being an active agent of global climate change (Robock, 2000; Robock & Mao, 1995) and imposing adverse effects on local environments (Delmelle et al., 2002). Volcanic SO_2 emissions impact atmospheric composition, which in turn can influence the environment at a range of scales, through acid rain production (Hoffman et al., 1985) and the formation of aerosols which have regional, if not global, climatic implications, (King et al., 1992; Robock 2000). Furthermore, quantification of SO_2 emissions provides an insight into volcanic processes (e.g. Sutton et al., 2001), which can lead to the forecasting of potentially hazardous events.

Of all the volcanic gases, SO_2 is the most readily detected due to its relatively high abundance in plumes compared to very low concentrations in the ambient atmosphere. Remote sensing offers a means to quantify volcanic emissions, particularly where active sampling is too dangerous or impractical. Satellite-based instruments are able to monitor eruptive activity over large spatial domains, whereas ground based monitoring techniques are more specifically tailored for individual systems. SO_2 lends itself to detection by remote methods due to its distinct absorption features in both the ultraviolet (UV) and thermal infrared (TIR) regions of the electromagnetic spectrum. Although satellite-based instruments are rarely designed for the sole purpose of volcano monitoring, a range of sensors have been shown to be useful in the detection of volcanic gas. Three *National Aeronautics and Space Administration* (NASA) instruments are used in this study — the Total Ozone Mapping Spectrometer (TOMS) (Krueger et al., 1995) and its successor, the Ozone Monitoring Instrument (OMI) (Levelt et al., 2006) which are designed to measure global ozone concentrations and the Moderate Resolution Imaging Spectroradiometer (MODIS) (King et al., 1992; Salomonson et al., 2002) has 36 wavelength bands with which to observe land, oceanic and atmospheric processes.

All three of the aforementioned sensors have instrument-specific advantages and limitations with regard to volcanic SO_2 measurement (Table 1). For example, TOMS provides an extensive dataset from 1979 until the end of 2006 (Carn et al., 2007). However, the spatial resolution (39×39 km^2 at nadir) of the instrument is coarse when compared to OMI (13×24 km^2 at nadir) and MODIS (1 km^2 at nadir) and therefore limits its usefulness to large plumes. OMI continues the TOMS dataset with a finer spatial resolution and improved retrieval algorithms, with an order of magnitude increase in sensitivity from ~4 to 0.4 Dobson Units (DU) (Krotkov et al., 2006). Both UV instruments use the reflection of sunlight from the Earth back to the sensor to perform retrievals and are therefore limited to operating in daylight hours. Furthermore, at high latitudes, long path lengths reduce the accuracy of the SO_2 retrieval and interference due to the presence of ozone, ash and ice can increase light scattering and therefore affect retrieval accuracy (Bluth et al., 1993). The MODIS instrument has a considerably finer resolution and the added benefit of both day and night

* Corresponding author. Department of Earth Sciences, University of Bristol, Wills Memorial Building, Queen's Road, Bristol, BS8 1RJ, UK. Tel.: +44 1179545427.
E-mail address: hethomas@mtu.edu (H.E. Thomas).

0034-4257/$ – see front matter © 2009 Elsevier Inc. All rights reserved.
doi:10.1016/j.rse.2009.02.019

Table 1
Summary of main features of the Earth Probe (EP) TOMS, OMI and MODIS instruments used in this study.

Name	Nadir spatial resolution	Launch year	Spectral range	Advantages	Limitations
TOMS	39×39 km^2 (EP) *Diamond*	1979	308–360 nm (UV)	•Very long historical record	•Poor spatial resolution. •Daytime only •Non-tessellated pixels •Ash, ice and ozone interference
OMI	13×24 km^2 *Normal Mode* 13×12 km^2 *Zoom in mode* *Trapezoid*	2004	270–500 nm (Vis/UV)	•High spatial resolution •Higher SO_2 sensitivity cf. TOMS	•Daytime only •Ash, ice and ozone interference
MODIS	1×1 km^2 *Square*	1999	0.64–14.3 μm (IR/Vis)	•Day and night functionality •V. high spatial resolution •High temporal resolution	•Strong interference from ash, aerosols and ice

The spatial resolution given is the smallest possible pixel size, at nadir.

time functionality although retrievals are hampered when the underlying Earth's surface is cool (Prata et al., 2003; Rose et al., 2003). A number of studies exist where more than one sensor is used to attempt to quantify eruptive SO_2 (e.g. Rose et al., 2003; Schneider et al., 1999), although the direct relationship between the sensors remains poorly constrained.

The intent of this study is to outline a methodology which allows the direct comparison of SO_2 retrievals from two UV (TOMS and OMI) and one TIR (MODIS) satellite oriented sensors based on the original method of Kearney et al. (in review). Results of a comparison performed on the October 22–30, 2005 eruption of the Sierra Negra volcano, Galápagos Islands are presented. Satellite images from October 23, the first full day of eruption, were used in this study. Retrievals by the three instruments using various acquisitions were conducted and the results compared both spatially and quantitatively.

1.1. MODIS

Two identical MODIS instruments aboard the NASA Aqua and Terra platforms currently orbit the Earth in sun-synchronous, near polar, circular orbits (http://modis.gsf.nasa.gov). MODIS wavelength bands span the visible (VIS) and thermal infrared wavelengths (TIR) (King et al., 1992) and it is therefore capable of detecting a number of volcanic species due to absorption over infrared wavelengths including ash, sulphates and SO_2 (Watson et al., 2004). SO_2 has two absorption signals in the TIR — one at 7.3 μm (MODIS band 28) and the other at 8.6 μm (MODIS band 29) (Fig. 1).

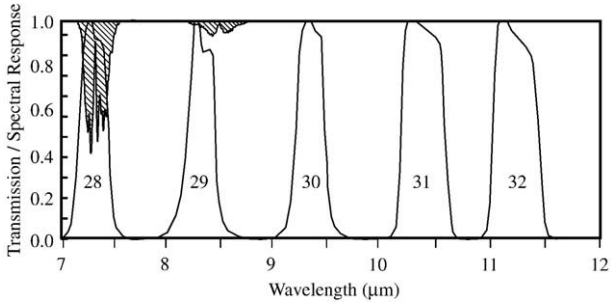

Fig. 1. Transmission spectrum of SO_2 (shaded) and the Moderate Resolution Imaging Spectroradiometer (MODIS) spectral response functions for channels 28–0 overlain. The SO_2 absorption only affects channel 28 (7.3 μm) more strongly than channel 29 (8.6 μm). Figure adapted from Watson et al., 2004, Fig. 1.

Table 2
Overpass times of the instruments used in this study.

Sensor (platform)	Time image acquired UTC (local)
MODIS (Terra)[a]	0355 (2155)
MODIS (Terra)	1620 (1020)
TOMS (Nimbus 7)	1800 (1200)
MODIS (Aqua)	1910 (1310)
OMI (EOS Aura)	1927–2109 (1327–1509)

[a] Indicates that this retrieval was not used in the study due to the inappropriate timing with respect to the other sensors and the small portion of the plume imaged due to the volcano location close to the swath edge.

The absorption at 7.3 μm is significantly stronger of the two, but its usefulness is constrained by the presence of atmospheric water vapour which is also a strong absorber at this wavelength (Prata et al., submitted for publication). The 7.3 μm retrieval is therefore limited to plumes in the upper troposphere and stratosphere where the atmosphere is relatively dry (Prata et al., 2003). The weaker 8.6 μm feature has more value when monitoring low altitude, passively degassed plumes (Realmuto et al., 1997) although is compounded by interference from other species such as ash, ice and aerosols (Watson et al., 2004).

1.1.1. 7.3 μm retrieval

A brief outline of the retrieval is given here, but for a more detailed explanation see Prata et al., 2003. The basic model can be expressed as:

$$I - I_\alpha = (1 - \tau_s)(B_s - I_\alpha) \quad (1)$$

where I is the measured radiance at 7.3 μm, I_α the radiance at 7.3 μm for normal atmosphere, τ_s the SO_2 transmittance and B_s the Planck radiance for the cloud at temperature T (Prata et al., 2003, submitted for publication). The temperature difference between the measured radiance and the SO_2-free radiance (as derived from the inverse Planck function) can be related to transmittance by:

$$\Delta T = \alpha + \beta(1 - \tau_s) \quad (2)$$

where α and β are estimated parameters and are a function of atmospheric state and temperature of the SO_2 cloud.

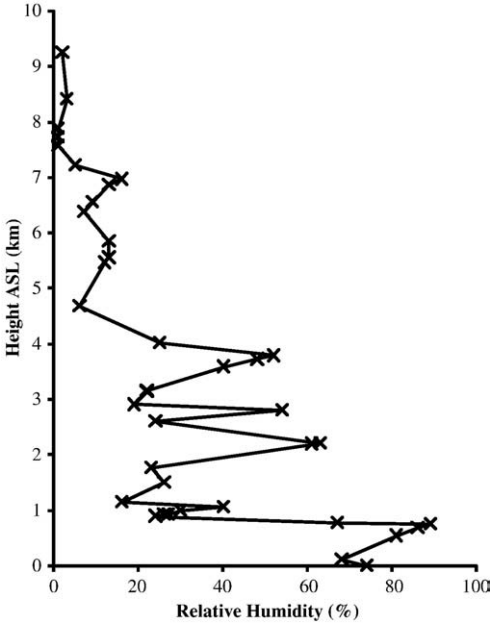

Fig. 2. Graph of the mass mixing ratio of water vapour in the atmosphere with altitude. Data from the radiosonde launched at 1200 local time, from the nearby San Cristobal Island, the nearest station to Sierra Negra. Data from: http://weather.uwyo.edu/upperair/sounding.html.

The retrieval utilises MODIS channels 27 (6.27 μm) and 31 (11.03 μm) to estimate the contribution of background atmosphere to the at-sensor radiance, as these channels are unaffected by the presence of SO_2. As the SO_2-free radiances of channels 27, 28 and 29 vary approximately linearly with wavelength, an estimate of radiance when SO_2 is absent at 7.3 μm (channel 27), $I_{\alpha,}$ can be determined. The measured brightness temperature at 7.3 μm is lower than the interpolated value when SO_2 is present. The difference between predicted and actual temperatures is therefore assumed to be directly related to the quantity of SO_2.

1.1.2. 8.6 μm retrieval

The original model of Realmuto et al. (1994), based on the Moderate Resolution Atmospheric Transmission (MODTRAN) radiative transfer code (Berk et al., 1984) was initially developed for retrievals of passively degassed plumes using the Thermal Infrared Multispectral Scanner (TIMS). It was later adapted for use with the MODIS and the Advanced Spaceborne Thermal Emission and Reflection Radiometer (ASTER) sensors (Realmuto, 2001). MODTRAN has proven useful for both passive degassing and explosive measurements (Watson et al., 2004).

In the model, the at-sensor radiance is expressed as:

$$L_s = \left[\varepsilon_g B\left(T_g\right) + \left(1-\varepsilon_g\right)L_d\right]t_a + L_u \quad (3)$$

where L_s is the at sensor radiance, ε_g the ground emissivity, B the Planck function, T_g the ground temperature, L_d the downwelling radiance, t_a the spectral transmittance of the atmosphere and L_u the upwelling radiance (Realmuto et al., 1994). The atmosphere is modelled as isothermal layers, each acting as either a source or emitter so that the terms L_s, L_d and L_u represent the total emission and absorption of all layers (Realmuto & Worden, 2000). MODTRAN computes $L_u(\lambda)$, $L_d(\lambda)$, and $t_a(\lambda)$ from atmospheric profiles of pressure, temperature, humidity and atmospheric constituents (Realmuto et al., 1994).

Eq. (3) is solved for T_g for the channels whose radiance is unaffected by the presence of SO_2, namely MODIS bands 30–32. This yields the 'true' ground temperature which can be compared to the

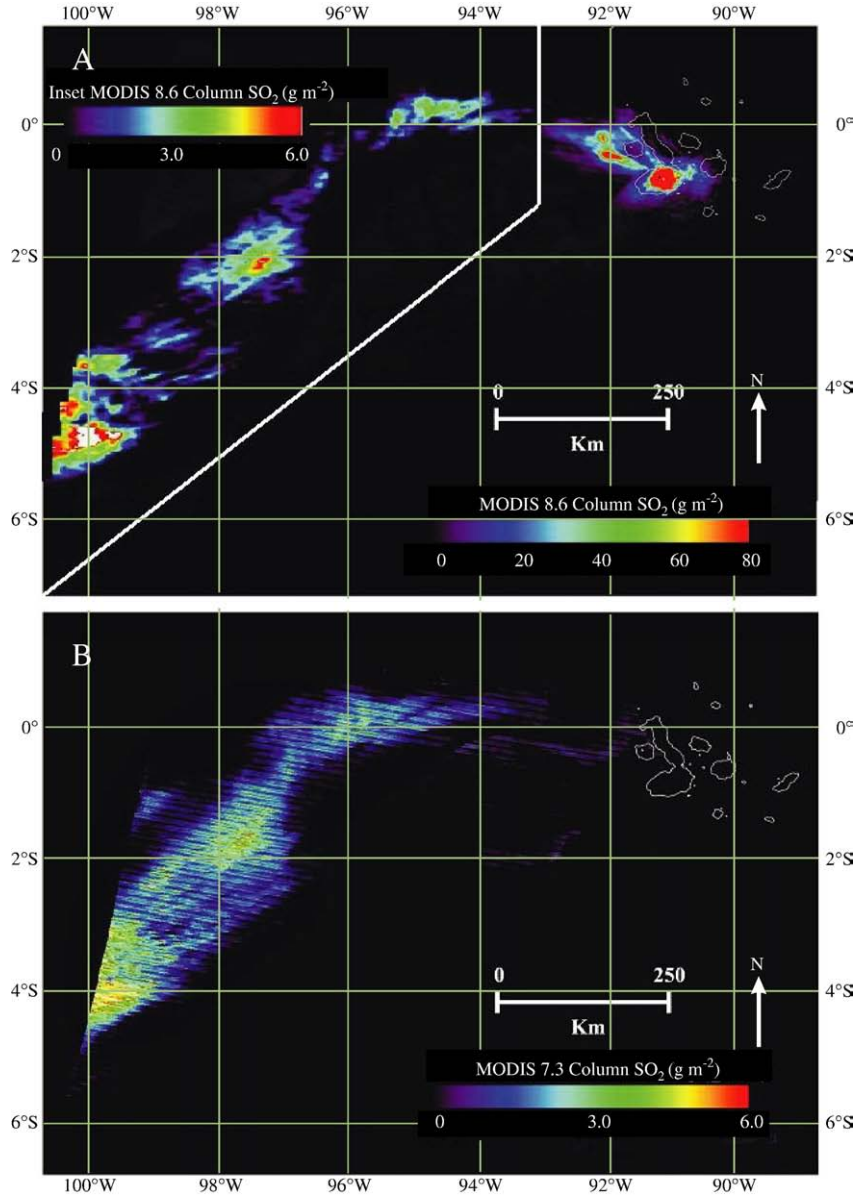

Fig. 3. MODIS retrievals acquired on October 23, 1620 UTC (1020 local time). A) shows the retrieval of the plume by MODIS using the 8.6 μm method. Two colour scales are used to account for the large disparity in values between the region over the islands and the rest of the plume. B) shows the retrieval from the same MODIS overpass, using the 7.3 μm method.

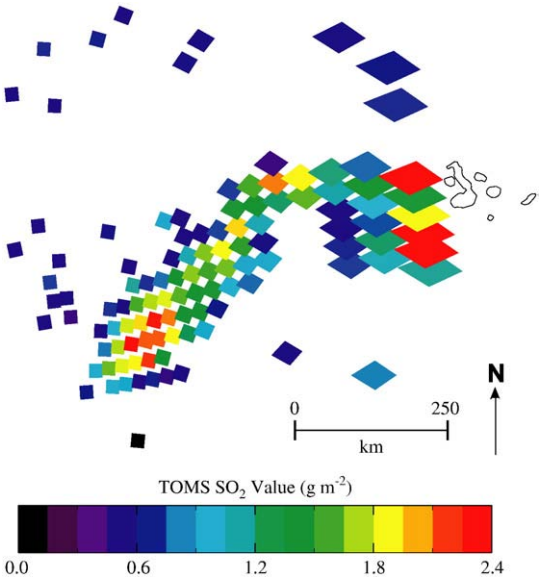

Fig. 4. Total Ozone Mapping Spectrometer (TOMS) SO_2 retrieval captured at approximately 1800 UTC (midday local time). Only pixels above the TOMS detection threshold of 0.4 g m^{-2} are shown.

'apparent' ground temperature which results from solving Eq. (3) for channel 29 (8.6 μm). When SO_2 is present, the apparent temperature is lower than the true ground temperature due to the absorption of ground leaving radiation by the gas. The difference between the two temperatures is a function of SO_2 concentration (Watson et al., 2004).

1.1.3. Retrieval methodology

MODIS level 1B raw data was obtained via NASA's Level 1 Atmosphere Archive and Distribution System (http://ladsweb.nascom.nasa.gov/). For the 7.3 μm retrieval, MODIS level 1B data was processed to produce both an image of the plume and data containing SO_2 concentrations across the scene. This analysis required an input of prescribed plume altitude. The MODIS 8.6 μm retrieval is less straightforward due to the MODTRAN radiative transfer code requiring a number of user inputs such as plume altitude, thickness, local atmospheric conditions and properties of the underlying surface (Berk et al., 1984). The retrieval was performed using the MAP_SO2 programme (Realmuto & Worden, 2000) which provides a graphical user interface to the MODTRAN algorithm. The programme requires the input of georeferenced MODIS data with radiance values for channels 29–32. A decorrelation stretch was performed to create an

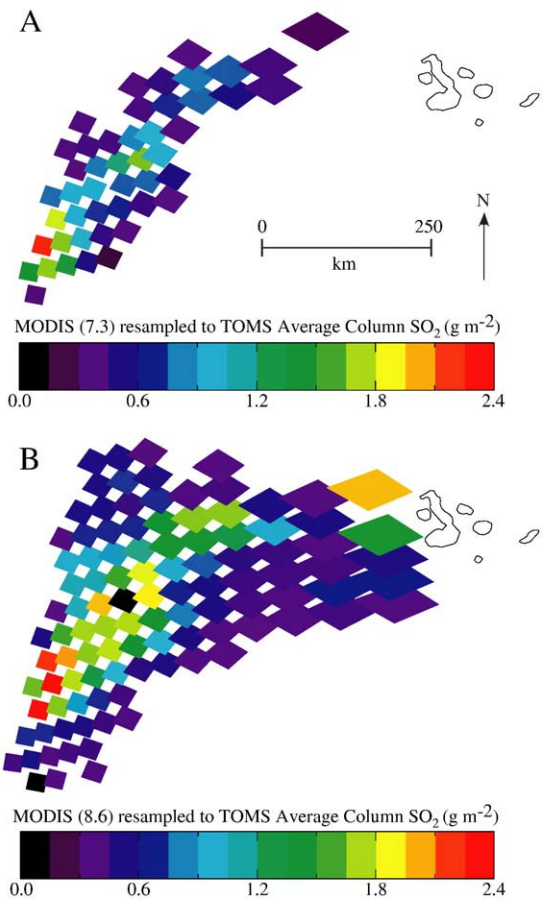

Fig. 6. MODIS retrievals at 1620 UTC resampled to TOMS pixel geometry. A) MODIS 7.3 μm retrieval resampled, B) MODIS 8.6 μm retrieval resampled.

image in which SO_2 can be more easily distinguished from the background in order to allow better delineation of the plume (Alley, 1996; Gillespie et al., 1986).

MODTRAN calculates the SO_2 concentration in the plume by utilizing models of absorption bands for 12 different gas molecules (SO_2 included). The strength of the absorption of the ground-leaving radiance is a function of SO_2 concentration, atmospheric pressure at the plume altitude, temperature contrast between the plume and ground and the plume thickness (Realmuto et al., 1997). As this is an under-determined problem, the following additional parameters are required by the algorithm to compute SO_2 concentration. An atmospheric profile

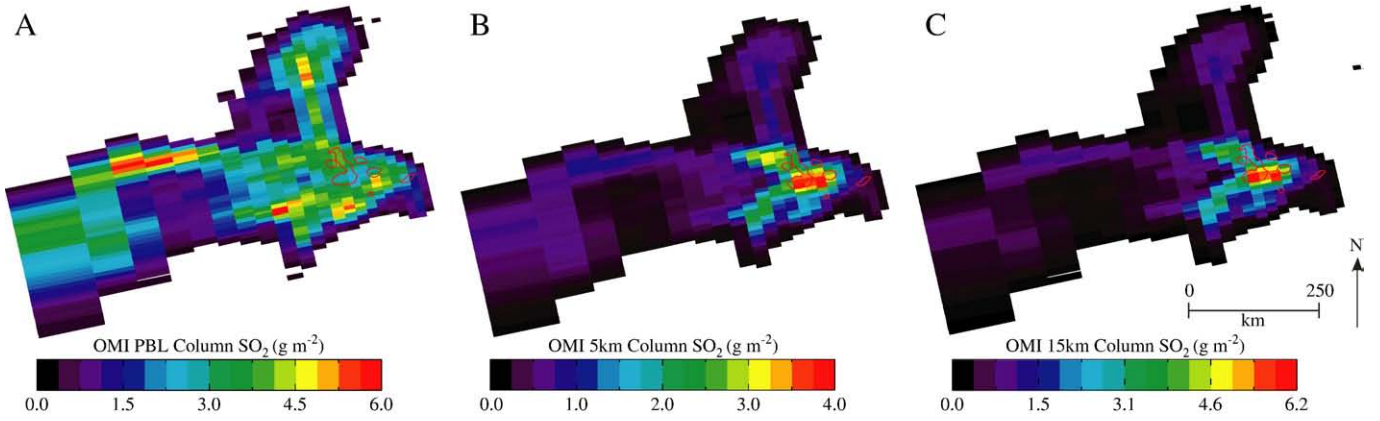

Fig. 5. The three Ozone Monitoring Instrument (OMI) retrievals of the Sierra Negra plume. Images captured between 1927 and 1931 UTC (1327–1331 local time) and processed using the linear fit algorithm for three different vertical profiles: A) Planetary Boundary Layer (PBL) (0–3 km), B) 5 km (5–10 km), C) 15 km (10–15 km).

containing information on altitude, pressure, temperature and relative humidity is pre-loaded into the MAP_SO2 interface. In this case the only local atmospheric data was a radiosonde station on San Cristobal Island. The data was downloaded from: http://weather.uwyo.edu/upperair/sounding.html. The plume altitude and thickness are determined by the user and also entered into the interface. In this study, the plume altitude was determined from literature (GVN, 2005; Geist et al., 2008) and HYSPLIT modelling (Draxler & Rolph, 2003) as 3 km close to the vent, lofting to 12 km at its most westerly extent. The vertical plume thickness is assumed by the model to be 1 km throughout. The temperature and emissivity of the ground in SO_2 free conditions are required to calculate the 'true' ground temperature. These are computed within MAP_SO2 by defining a region representative of the ground beneath the plume where the plume is not present. The user then selects regions of the plume and run the MODTRAN algorithm to generate a map of SO_2 concentration of the entire plume.

1.2. TOMS

Since 1978 the four TOMS instruments provide a near continuous dataset up to late 2005 (http://toms.umbc.edu/). TOMS detects backscattered radiation in the near-ultraviolet region of the electromagnetic-spectrum and measures in six wavelength bands from 308 nm to 360 nm (Krotkov et al., 1997). A Sulphur Dioxide Index (SOI) is computed to indicate the presence or absence of SO_2 by comparison with pre calculated radiances (Bhartia, 2003; McPeters et al., 1998). Pixels with an elevated SOI are then processed for SO_2 content.

The SO_2 retrieval is based on the Residual Model of Krueger (1983) which was later replaced by the Linear Model (Kerr Algorithm) (Kerr et al., 1980; Krotkov et al., 1997; Krueger et al., 2000). The Linear Model assumes that solar radiation is attenuated by absorbing species according to Beers law so that:

$$I(\lambda) = I_0(\lambda) exp[-\tau_a(\lambda)] \quad (4)$$

where $I(\lambda)$ is the intensity of radiation at wavelength λ, τ_a is the absorption optical path through the atmosphere and I_0 is the expected intensity for a clear atmosphere. By making assumptions about the spectral dependence of I_0 and making retrievals simultaneously at four TOMS wavelengths, the at sensor radiance can be related to the log of the reflectance of the atmosphere ($N(\lambda)$) by the following expression:

$$N(\lambda) = -100 log[(I(\lambda) / F_0(\lambda)) \cos(SZA)] \quad (5)$$

in which $I(\lambda)$ is the upwelling atmospheric radiance, $F_0(\lambda)$ the solar spectral irradiance and SZA the solar zenith angle. The version of the algorithm in this study is the most recent (http://toms.umbc.edu/), which improves upon earlier versions by utilising new temperature and ozone profiles, which are dependent on month, latitude and total ozone.

1.3. OMI

The Linear Fit algorithm was used to process the OMI data and as with TOMS, the algorithm utilises the differential absorptions of ozone and SO_2. The algorithm measures backscattered UV (BUV) radiances at ten OMI wavelength bands between 310 and 360 nm and inputs the values into the TOMS Radiative Transfer Model (TOMRAD) forward model. The model computes the top of atmosphere (TOA) radiance for

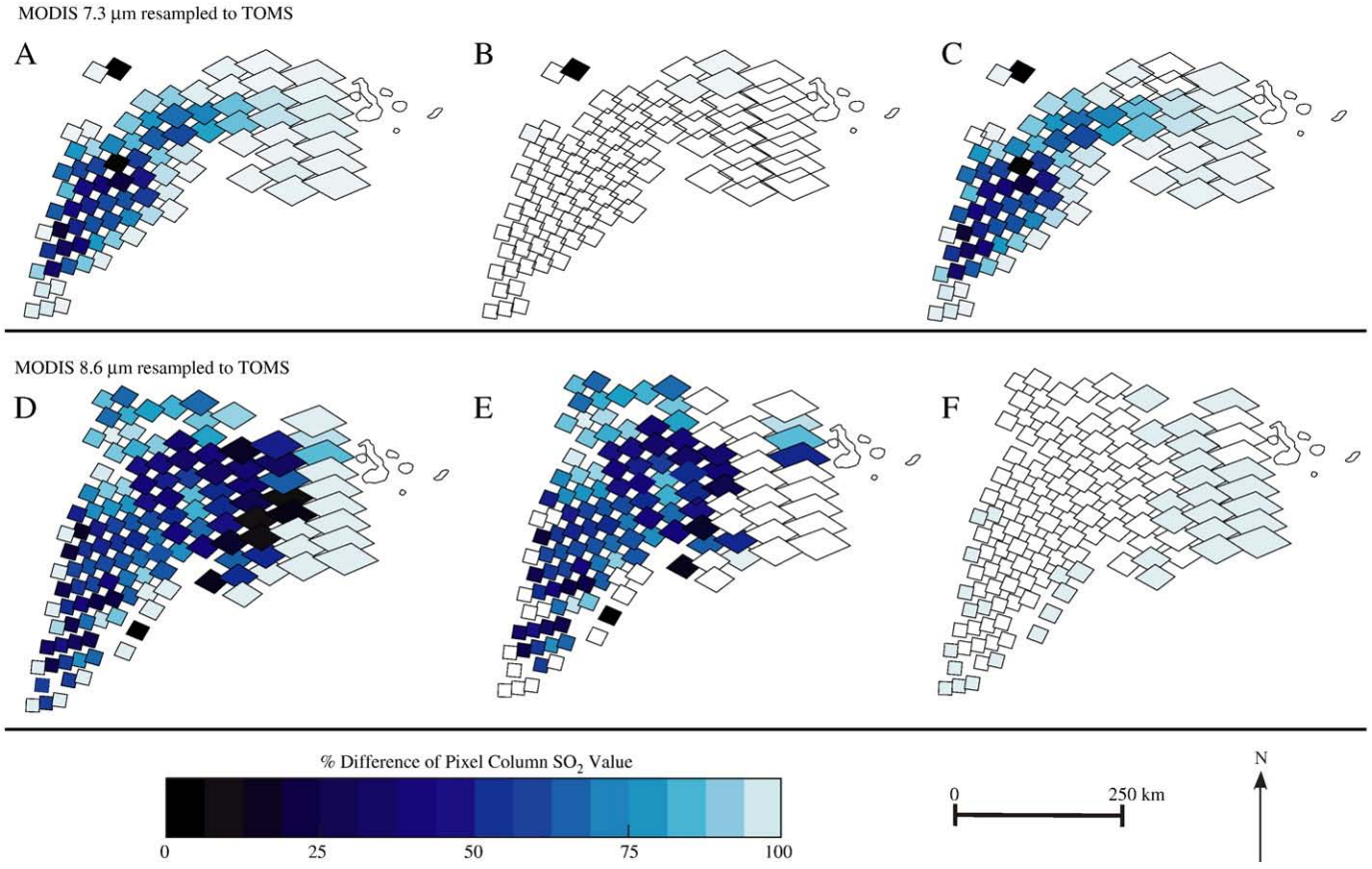

Fig. 7. Percentage difference maps between MODIS 7.3 µm and MODIS 8.6 µm retrievals acquired at 1620 UTC, resampled to TOMS pixels with the original TOMS data acquired at 1800 UTC. A) and D) show the absolute percentage difference, B) and E) the percentage difference where MODIS>TOMS values and C) and F) the percentage difference where TOMS>MODIS. White pixels indicate no data for each particular comparison.

each wavelength, and compares these to the measured values (Yang et al., 2007).

BUV radiances, I_m, are related to column ozone (Ω), SO_2 (Ξ), surface reflectivity (R) and modelled radiance (I) by the following relationship:

$$logI_m = logI(\Omega, \Xi, R) + \varepsilon \quad (6)$$

which, for the retrieval, is expressed as:

$$N_m = N((\Omega, \Xi, R) + \varepsilon_T \quad (7)$$

where N is a dimensionless value and ε_T the total of measurement and model errors. The variables Ω, Ξ and R are adjusted until the TOA radiances from the TOMRAD forward model match the measured radiances at the selected wavelength bands. The data contain three sets of results depending on the pre-defined plume altitude profile used in the retrieval. These are: the Planetary Boundary Layer (PBL, 0–3 km), 5 km (5–10 km) and 15 km (10–15 km). In this work the results from all three profiles are considered.

1.4. Case study selection

In order to perform a comparison of the three instruments an eruption which fulfilled a number of requirements had to be selected. These criteria included: near coincident acquisitions to minimise the time for plume motion between retrievals, a sufficiently large plume to allow the comparison of a number of pixels, little or no ash present which would interfere with the retrievals by absorption and scattering of radiation, and few clouds to provide a clear scene on which to perform retrievals.

The Galápagos Islands consist of at least 20 subaerial volcanoes (Munro & Rowland, 1996) with the younger, most active volcanism in the west of the region (Christie et al., 1992). The 2005 eruption of Sierra Negra, Galápagos Islands, began on October 22 at 2330 UTC (1730 local time) and was preceded by a seismic event earlier that day (Hall et al., 2005). Following an initial explosive phase, eye witnesses reported plume altitudes of over 10 km ASL (GVN, 2005; Geist et al., 2007). Initial analysis of MODIS imagery of the first full day of eruption (October 23) indicated a relatively cloud free scene, with a large, SO_2-rich plume making this a suitable target for instrument comparison. The overpass times of the three instruments are given in Table 2.

1.5. Issues involved in performing a comparison between sensors

1.5.1. Time lag between acquisitions

The aim of this study was to perform a comparison, on a pixel by pixel basis of three different methods by which volcanic SO_2 can be quantified using satellite imagery. An ideal scenario would be one in which all three instruments recorded at the same instance, thus comparing the plume at the same moment in time and space. As it is, there is a gap of 1 h 40 min between MODIS (Terra) and TOMS acquisitions, 3 h 5 min between MODIS (Terra) and OMI and 15 min between MODIS (Aqua) and OMI (Table 2). Large time differences allow for significant plume motion as estimates from the MODIS imagery suggest that the plume travelled about 660 km in the first 11 h, so initial velocity was estimated at ca. 60 km h^{-1}. This would change the spatial distribution of the plume and in some areas the plume may have moved by entire TOMS pixels or up to three OMI pixels which would invalidate a pixel scale comparison. The short 15 min time difference between the Aura and Aqua overpasses provides the best case scenario, although in this study the spatial limitations of MODIS restricts the comparison.

1.5.2. Effects of other species on the retrievals

Volcanic ash, sulphates, ice and water vapour can all have a significant impact on the retrieval of SO_2 by the MODIS retrieval methods (Watson et al., 2004). In this case, the plume was shown to be relatively ash poor by observation of visible MODIS imagery. However, the presence of sulphate aerosols and ice cannot be ruled out. The geographical location of the Galápagos Islands within the tropics implies that the atmosphere would be water-rich which is confirmed by radiosonde profile, showing a significant percentage of water up to ca. 7 km (Fig. 2). Water vapour masks SO_2 in the 7.3 μm retrieval as discussed previously and can also cause interference at 8.6 μm. The presence of ash, ice and sulphates affect both MODIS retrievals although the effects are generally greater on the 8.6 μm retrieval (Watson et al., 2004). Such species also have effects on the UV instrument retrievals. Thin layers of aerosols can result in overestimation by TOMS (Krueger et al., 1995) and different aerosol types have varying, and often complex effects (Thomas et al., 2005). Overestimation due to aerosols is variable with viewing angle, (Krueger et al., 1995). OMI suffers less than TOMS by interference as some species such as aerosols and other absorbing gases are accounted for in the TOMRAD forward model (Yang et al., 2007).

1.5.3. Dependence on plume altitude

All retrievals with the exception of TOMS, require an estimate of plume altitude, which subsequently affects the values of SO_2 retrieved. It is clear from the three different OMI retrievals (Fig. 5) that the chosen plume altitude plays an important part in the validity of the retrieval. In a scenario such as this, where plume altitude is thought to differ with distance from the vent, the instrument retrieval is compounded by choice of prescribed altitude profile.

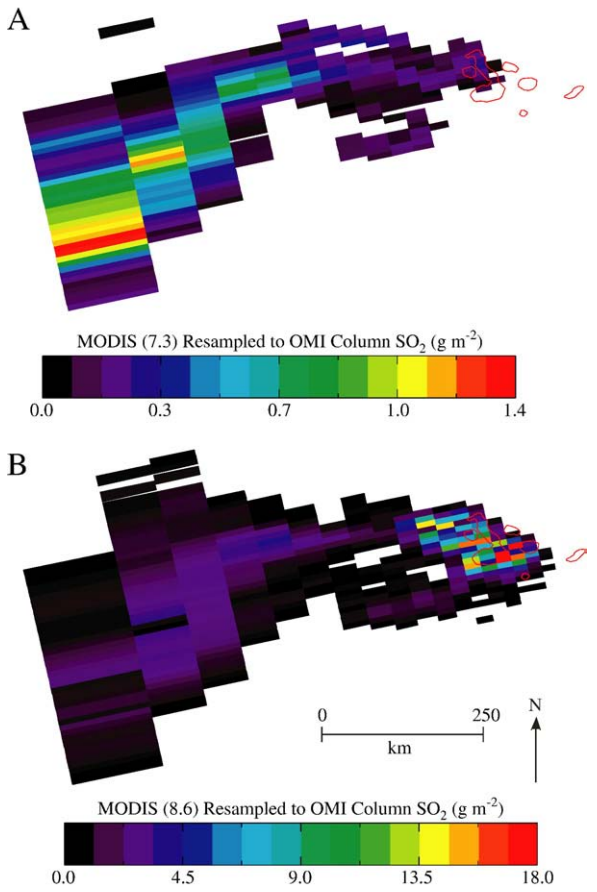

Fig. 8. MODIS retrievals from 1620 UTC acquisition resampled to OMI pixels from 1927–1931 retrieval. A) MODIS 7.3 μm retrieval resampled, B) MODIS 8.6 μm retrieval resampled.

Both MODIS retrieval methods are also altitude dependent. The MAP_SO2 interface allows the user to select altitude for each section of the plume retrieved and so variations in plume height can be accounted for, although problems still may result from inaccurate altitude estimates. The MODIS 7.3 μm retrieval requires an inputted altitude profile before the retrieval is performed. An inaccurate altitude, as with the OMI retrievals, can produce differences in SO_2 quantities.

1.5.4. Instrument error

Error resulting from uncertainty in the validity of the retrieval algorithms should also be considered. Prata et al. (2003) offer a complete discussion of error in the MODIS 7.3 μm method, and estimate that total error varies from 5% to 20% depending on the individual setting. MODIS 8.6 μm retrievals have been estimated as up to 17% in error due to uncertainties in input parameters such as plume altitude and thickness, atmospheric conditions and ground emissivity (Realmuto and Worden, 2000). The MAP_SO2 procedure involves some user subjectivity such as arbitrarily defining the plume region and selecting a representative background surface which can result in variable outcomes between users.

The OMI Linear Fit (LF) algorithm is thought to be robust up to 0.85 g m^{-2} and is known to overestimate SO_2 where concentrations are above ~1.4 g m^{-2} due to the non-linear effect, which is described in detail by Krotkov et al., 2006 and Yang et al., 2007. The error can be up to 70% for concentrations of 11.4 g m^{-2} and so in this case study, the retrieval may fail close to the vent where concentrations are highest.

A full analysis of TOMS retrieval errors is given by Krueger et al. (1995) and shows that error results from changing scan angle, instrument calibration, absorption coefficient inaccuracies, algorithm error as well as random errors. Algorithm errors are estimated by Krueger et al. (1995) to be ± 3% for 2.9 g m^{-2} although where scan and satellite zenith angles are large, error can be as much as ± 15%. It should therefore be acknowledged when performing an instrument comparison, that all three sensors are subject to error, which in some instances may be large.

2. Results

Fig. 3 shows the retrieval of the plume using the two MODIS methodologies acquired at 1620 UTC on October 23, 2005. The 8.6 μm retrieval is split due to the large difference in scales of the retrieval, which showed large SO_2 burdens directly over the islands, whereas the 7.3 μm retrieval does not image this low-level SO_2. The two retrievals do show similar magnitude results for the westerly, higher altitude part of the plume.

The plume imaged by TOMS at approximately midday local time (1800 UTC) is shown in Fig. 4. Krueger et al. (1995) estimate the standard deviation due to background noise for the SOI method to vary from 0.16 g m^{-2} at nadir to 0.13 g m^{-2} at the swath edge. In order to eliminate irrelevant background pixels, the minimum value plotted was therefore set to the mean 3σ value of 0.44 g m^{-2} (3σ is

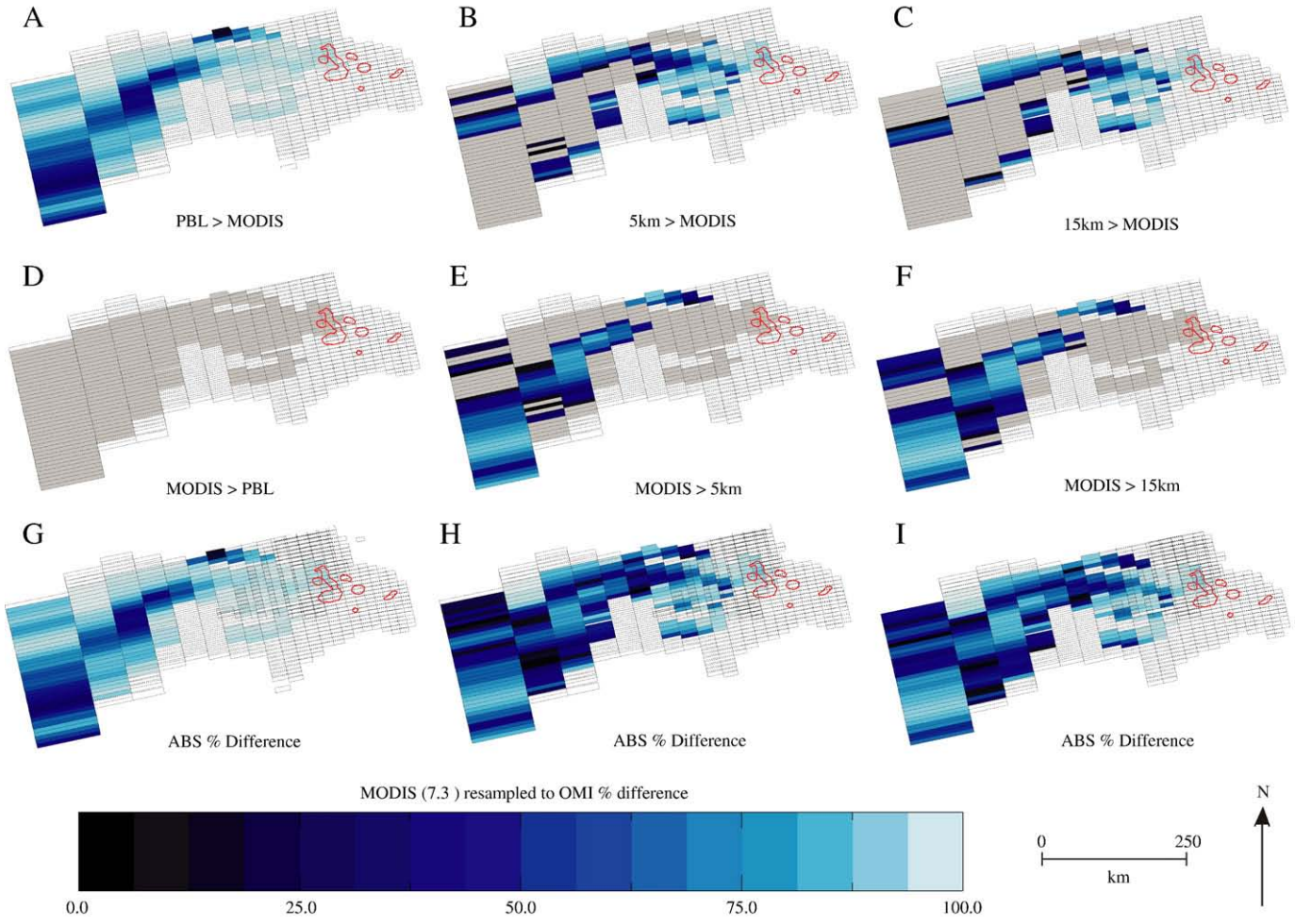

Fig. 9. Percentage difference maps between the MODIS 7.3 μm retrieval acquired at 1620 UTC resampled to OMI pixels and the original OMI data from the 1927–1931 retrieval. A, B and C show values where OMI>MODIS, D,E & F where MODIS values>OMI and G, H and I give the absolute % differences. Pixels in grey indicate where the other sensor is larger is larger (for images A–F) and unfilled pixels are those retrieved by OMI but where the MODIS resampled values show no data.

suggested by Carn et al., 2007 as a suitable threshold for OMI imagery). Fig. 5 shows the retrievals of the plume by OMI, calculated using the three pre-determined plume altitude profiles. On initial inspection it appears that the distribution of SO_2 from the 5 km and 15 km retrievals approximates that of MODIS and that these results are of a similar order of magnitude. Again, only pixels above the 3σ values, as calculated by Krotkov et al. (2006) were plotted in an attempt to eliminate background noise. These are 0.017 g m^{-2} and 0.026 g m^{-2} for the 15 km and 5 km retrievals respectively. No pre-determined value exists for the PBL retrieval using the Linear Fit algorithm and so a value of 0.14 g m^{-2} was chosen to best represent the plume extent.

The pixel size and shape of the three instruments vary significantly and also increase in size with viewing angle. To account for this, and therefore allow a direct comparison, MODIS pixels were resampled to the geometry and dimensions of the UV pixels using the method originally used by Kearney et al. (in review) to compare MODIS with TOMS. The method selects all MODIS pixels which lie within the spatial boundaries of each UV pixel and sums the total SO_2 within any one pixel. These totals are converted to concentration by dividing by the pixel area. For this, thresholds to eliminate pixels which were below the detection limits of the MODIS retrievals (and therefore considered as noise) were applied. These are 0.057 g m^{-2} for MODIS 7.3 μm (Crisp, 1995) and 1.0 g m^{-2} for MODIS 8.6 μm as determined for the MODTRAN retrieval by Henney et al. (in review). From this, pseudo- TOMS and OMI images were created with MODIS data.

The resampled TOMS images are shown in Fig. 6. It should be noted that the resampled MODIS images do not extend as far west as the original TOMS retrieval as the edge of the MODIS swath was reached. Most noticeably, the MODIS retrievals differ from the original TOMS retrieval in the area over the islands. This is expected in the MODIS 7.3 μm case where little SO_2 is seen due to its low altitude. However, there is also a large discrepancy in the values of the original TOMS retrieval and those of MODIS 8.6 μm in the TOMS swath closest to the islands. TOMS appears to have retrieved higher values than those of MODIS in this area. The discrepancies and similarities between the retrievals can be seen more clearly in the percentage difference map (Fig. 7). From these, TOMS almost always retrieved higher values than the MODIS 7.3 μm retrieval, although the two retrievals are within 25% difference in a significant portion of the high part of the plume. The MODIS 8.6 μm retrieval values however, almost always exceed those of TOMS. The best correlation between the two methods is seen over the westerly bulk of the plume with over half the total pixels matching within ±25%, with some regions in the most easterly swaths showing much larger percentage deviations. This could be due to error in TOMS measurements at these large viewing angles. A significant number of pixels at the plume edge also show TOMS values exceeding those of MODIS. This effect is due to some TOMS pixels only being partially covered by MODIS pixels during the resampling process.

Fig. 8 shows the results of resampling MODIS to the OMI pixels. Due to the larger field of view of OMI compared to MODIS, OMI recorded a larger spatial extent of the plume, in particular, heading

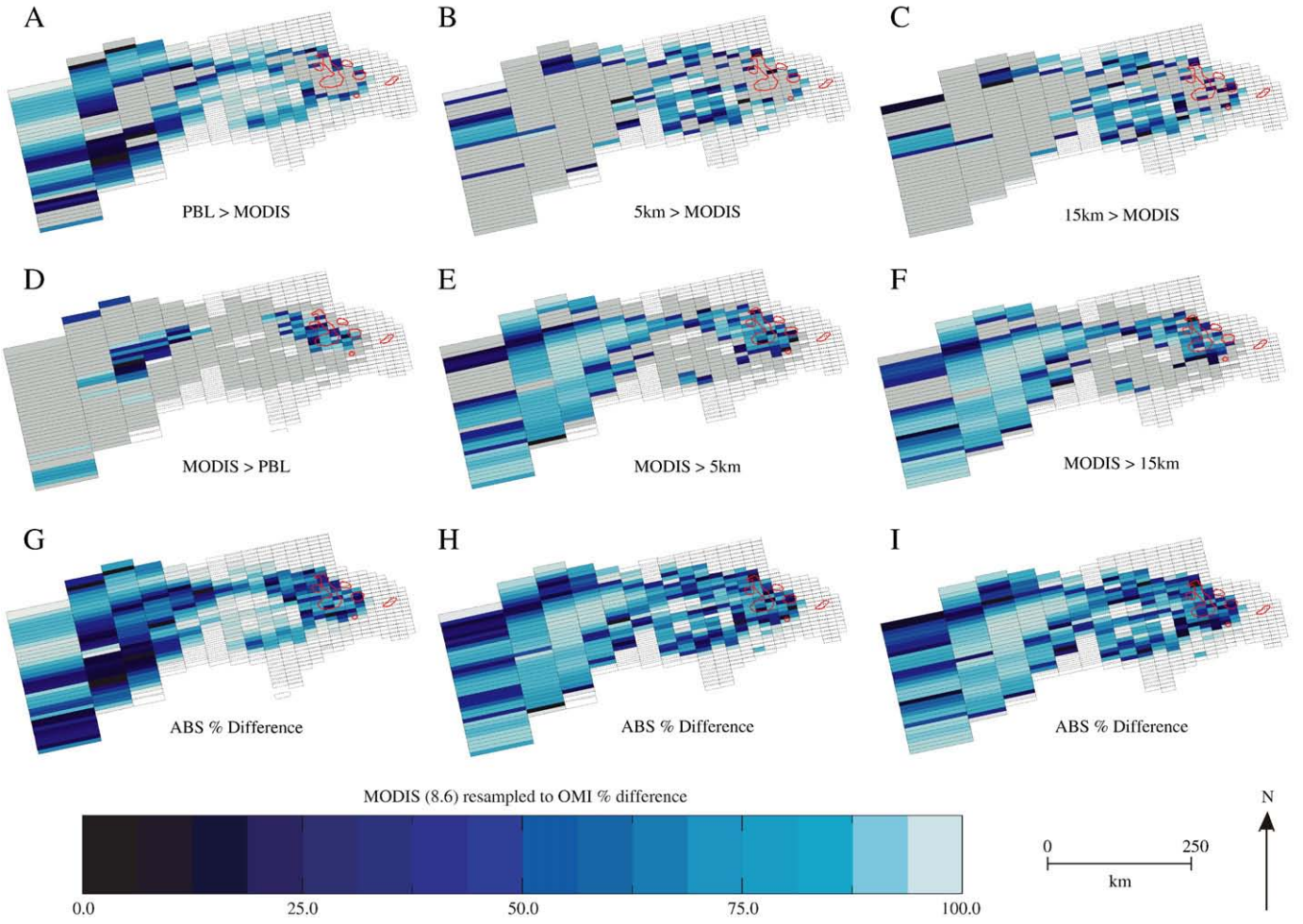

Fig. 10. Percentage difference maps between the MODIS 8.6 μm retrieval acquired at 1620 UTC resampled to OMI pixels and the original OMI data from the 1927–1931 retrieval. As before, A, B and C show values where OMI>MODIS, D,E and F where MODIS values>OMI and G, H and I give the absolute % differences. Pixels in grey indicate where the other sensor is larger (for images A–F) and unfilled pixels are those retrieved by OMI but where the MODIS resampled values show no data.

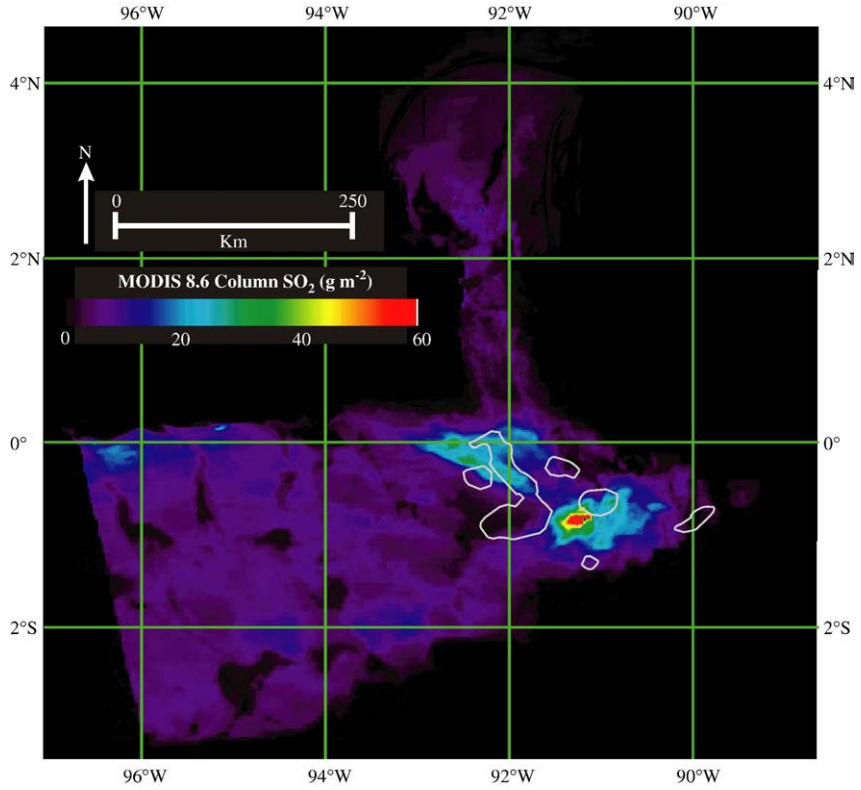

Fig. 11. MODIS Aqua overpass 8.6 μm retrieval of Sierra Negra plume at 1910 UTC (1310 local time).

north of the islands. For simplicity, the comparison figures only show OMI pixels which coincide with the MODIS retrieval. The MODIS 8.6 μm method shows a similar plume distribution to the OMI 5 km and 15 km retrievals, although values of the resampled MODIS 8.6 μm data are much higher than those of OMI 5 km and 15 km directly over the islands, yet are similar for the remainder of the plume. For the MODIS 7.3 μm method, values are generally much lower although they do begin to approximate the OMI values in the westerly region of the plume.

The comparison of MODIS 7.3 μm and OMI (Fig. 9) shows that OMI values are consistently much larger than MODIS in the low altitude region of the plume, which is expected due to masking of low-level SO_2 by water vapour. Most notably is a band travelling south-west where MODIS 7.3 μm values exceed those of OMI 5 km and 15 km. This band is also seen in the comparison of MODIS 8.6 μm to OMI (Fig. 10) which implies that the difference may be due to the plume changing position in the intervening time between retrievals. Another feature of note is the area of the plume directly south-west of the islands where OMI values exceed MODIS for all three OMI retrievals. This again could be due to changes in plume geometry over time or, as the MODIS 7.3 μm does not retrieve any SO_2 in this region, could be a result of water vapour masking SO_2 in the MODIS 8.6 μm retrieval (Watson et al., 2004).

A further feature of note is that to the east of the islands there is a semi-circular region of pixels which contain higher SO_2 concentrations for OMI compared to MODIS 8.6 μm values. This result implies that the OMI instrument is more sensitive to the presence of SO_2 at low concentrations such as at the plume extremities.

A second MODIS image was acquired on October 23 at 1910 UTC, which was spatially restricted as the islands were close to the swath edge, and therefore the instrument only retrieved a small portion of the plume. In this region, the plume is low level (<6 km), which is confirmed as the MODIS 7.3 μm method retrieved very little SO_2. The MODIS 8.6 μm retrieval is shown in Fig. 11 and indicates more dispersed plume morphology than the MODIS image taken at 1620 UTC. Furthermore, the 1910 UTC retrieval also views a part of the plume which headed north, which was missed by the MODIS 1620 UTC acquisition.

A comparison of the Aqua image with OMI is ideal in this case. The two sensors are a part of the NASA A-train: a sequence of Earth Observing Satellites trailing each other in orbit. As a result, Aqua overpasses consistently occur about 15 min prior to Aura (Schoeberl et al., 2006) and therefore the intervening time between retrievals is kept to a minimum. A comparison with TOMS was not conducted in this instance due to the small number of coincident pixels due to the TOMS data gap directly over the islands.

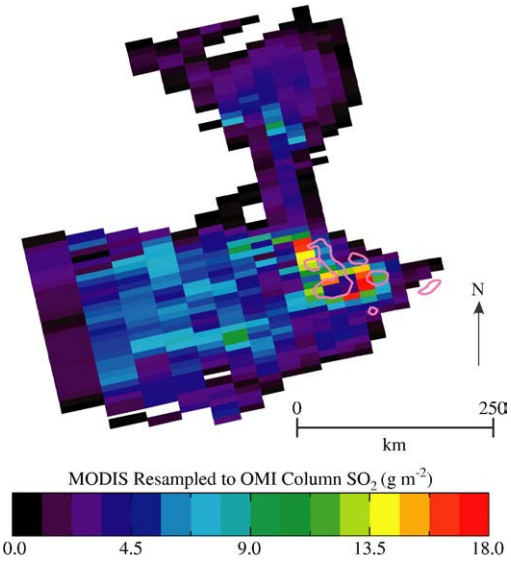

Fig. 12. MODIS 1910 UTC retrieval data resampled to OMI 1927–1931 retrieval pixel geometry.

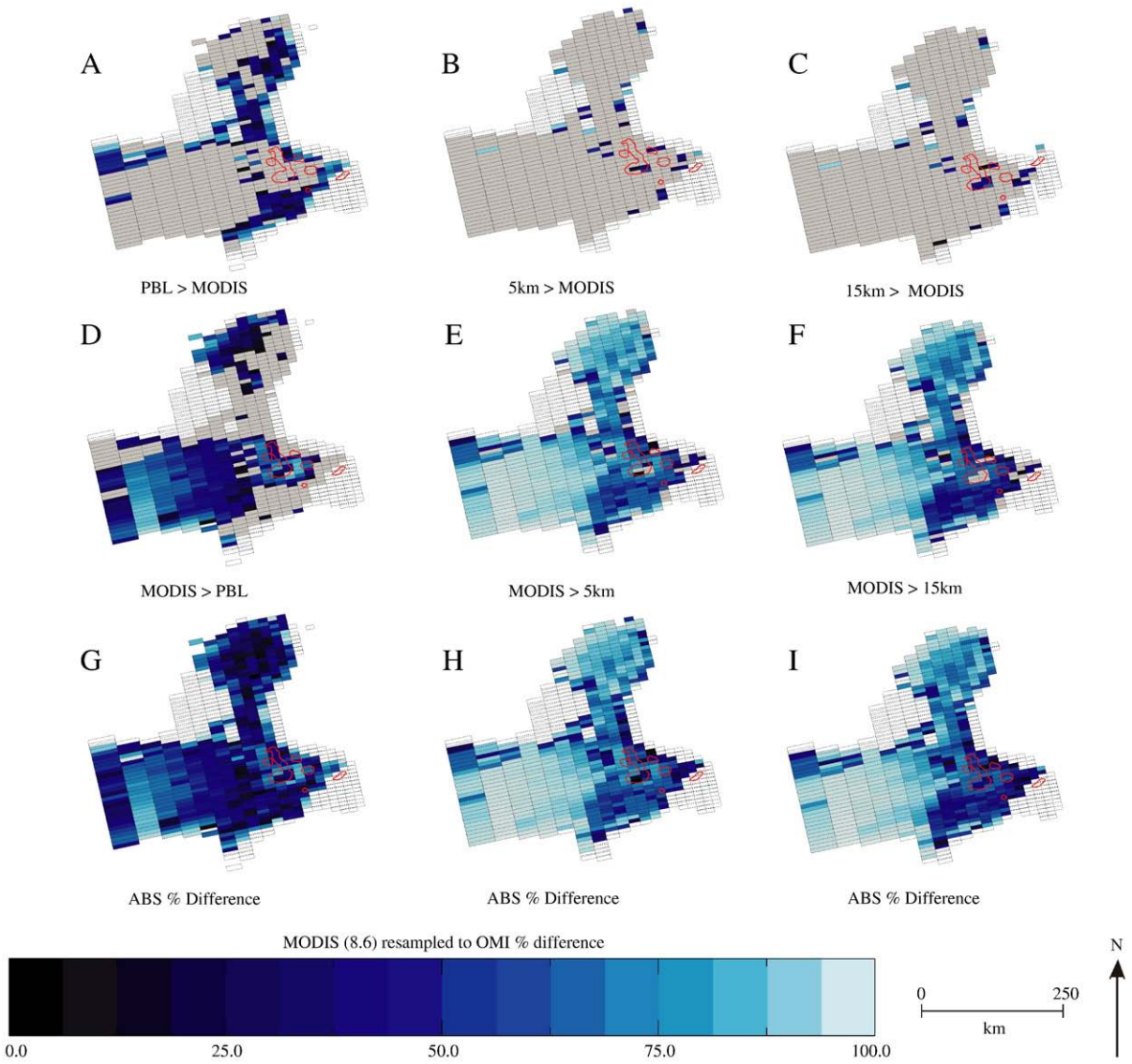

Fig. 13. Percentage difference maps between MODIS 8.6 μm retrieval acquired at 1910 UTC resampled to OMI pixels and the original OMI data from the 1927–1931 retrieval. A, B and C show values where OMI > MODIS, D,E and F where MODIS values > OMI and G, H and I give the absolute % differences. Pixels in grey indicate where the other sensor is larger is larger (for images A–F) and unfilled pixels are those retrieved by OMI but where the MODIS resampled values show no data.

The MODIS (Aqua) 8.6 μm results were resampled to the OMI (Aura) geometry as before, and the results are shown in Fig. 12. It should be noted that the three most westerly OMI scan lines are outside the MODIS field of view and therefore not used in the comparison. Furthermore, the fourth most westerly OMI swath was only partially overlain by MODIS pixels and so the MODIS resampled values may appear abnormally low in this case. The percentage difference maps show that that MODIS resampled values are almost always greater than those from OMI (Fig. 13). Exceptions to this are around the plume edges (particularly with the PBL comparison), which is likely to be due to the enhanced OMI sensitivity to SO_2. The region of plume which showed MODIS values being much lower than OMI for the comparison with the 1620 UTC image shows the opposite in this instance. It therefore seems likely that the original mismatch in retrievals was due to the plume having shifted south during the time between the MODIS (Terra) overpass and the OMI overpass. Both the original OMI and MODIS (Aqua) data imply that values in this region of disparity are relatively low from both sensors and thus small differences in absolute values could lead to seemingly large percentage discrepancy. The OMI PBL retrieval shows good correlation to MODIS in the region close to the islands, where the plume is at low altitude.

Table 3 presents the widely varying estimations of the total tonnages of for each of the retrieval methods. OMI PBL gives the highest total tonnage and also has the largest area of SO_2 containing pixels. This result is due to the retrieval being invalid for much of the plume as it is above the prescribed Planetary Boundary Layer altitude (0–3 km) used in the retrieval. The results are therefore erroneously large which significantly affects the validity of inter-sensor comparisons. The two MODIS 8.6 μm retrievals, although measuring over

Table 3
Total SO_2 tonnages for each retrieval method.

Retrieval method	Noise limit (g^{-2})	Total SO_2 (kt)	Retrieval Error	Area SO_2 (km^2)
MODIS 8.6 *(1620)*	1.0	833	~17%	1.9×10^5
MODIS 7.3 *(1620)*	0.057	59.9	5–20%	4.1×10^4
TOMS *(1800)*	0.44	332	18%	3.3×10^5
OMI PBL *(1930)*	0.14	1880	Up to 70% depending	9.3×10^5
OMI 5 km *(1930)*	0.026	377	on SO_2 concentration	8.9×10^5
OMI 15 km *(1930)*	0.017	401		9.2×10^5
MODIS 8.6 *(1910)*	1.0	1266	~17%	2.1×10^5

Time of acquisition given in brackets for each sensor.
All times are in UTC and all images were taken on October 23, 2005.

smaller areas, show large total SO_2 burdens. This is likely to be, at least in part, because the retrieval accounts for varying plume altitude and unlike the OMI 5 km and 15 km accounts for the dense, low level SO_2 as well as the higher part of the plume. The low tonnages of the MODIS 7.3 μm retrieval is due to the majority of the SO_2 lying within the water-rich lower atmosphere and is therefore obscured.

3. Conclusions and further work

This work has provided a direct comparison of the Moderate Resolution Imaging Spectroradiometer (MODIS), the Total Ozone Mapping Spectrometer (TOMS) and the Ozone Monitoring Instrument (OMI) retrievals of volcanic SO_2 from the Sierra Negra eruptive plume on October 23, 2005 at the pixel scale. The results from the study are variable and indicate that:

a) The total tonnages retrieved by the three sensors are variable and highly dependent on prescribed plume altitude and time of acquisition. MODIS 8.6 μm values exceed those of OMI 5 km and 15 km although are below the PBL retrieval values. The altitude variability of the plume used in this study implies the use of just one height profile may be invalid.
b) Spatial comparisons between the sensors are compounded by altitude differences as well as issues with geometry and individual instrument error.
c) The OMI instrument is likely to be more sensitive to SO_2 than MODIS. This was seen by OMI retrieving low SO_2 concentrations of plume to a more easterly extent than MODIS.
d) However, MODIS total tonnages are much greater than those of the UV instruments. This is partly due to MODIS retrieving the low level, highly concentrated plume but may also be a result of interference from other volcanic species such as ash and aerosols.
e) By using a number of retrievals the direction and speed plume motion as well as information about altitude profile can be inferred. In this instance, the plume is determined to be below 7 km where MODIS 7.3 μm was not able to retrieve any SO_2.

The methodology outlined here has the potential to be expanded to other SO_2 retrieving sensors such as the ASTER and the Atmospheric Infrared Sounder (AIRS). Incorporating more sensors in to the comparison would permit a better understanding of each sensors strengths and weaknesses and also the relationships between retrievals. To account for temporal discrepancies between acquisitions, forward modelling in regions where the plume speed and direction are well determined (from wind speed data) could be used to overlay images to simulate same-time acquisitions. By improving upon and extending the cross sensor comparisons, the development of more robust retrieval schemes for both these and a range of other sensors and will permit the more accurate quantification of global volcanic SO_2 from satellite-based sensors.

Acknowledgements

The authors would like to thank Peter Webley, Ken Dean and an anonymous reviewer for their suggestions from which this manuscript benefited greatly. Thanks also to Vince Realmuto and Fred Prata for provision of SO_2 retrieval programs and to the members of the OMI science team for providing information and data.

References

Alley, R. E. (1996). *Algorithm Theoretical Basis Document for Decorrelation Stretch, Version 2.2.*
Berk, A., Bernstein, L. S., & Robertson, D. C. (1984). *MODTRAN: A medium resolution model LOWTRAN-7. Tech. Rep. GL-TR-89-0122* Hanscom AFB, MA: Geophys. Lab.
Bhartia, P. K. (2003). TOMS V8 algorithm theoretical basis document. accessed on 10.12.2008 from. http://toms.gsfc.nasa.gov/version8/v8toms_atbd.pdf
Bluth, G. J. S., Schnetzier, C. C., Krueger, A. J., & Walter, L. S. (1993). The contribution of explosive volcanism to global atmospheric sulphur dioxide concentrations. *Nature*, *366*, 327—329.
Caltabiano, T., Romano, R., & Budetta, G. (1994). SO_2 flux measurements at Mount Etna (Sicily). *Journal of Geophyical Research*, *99*(D6), 12809—12819.
Carn, S. A., Krotkov, N. A., Yang, K., Hoff, R. M., Prata, A. J., Krueger, A. J., et al. (2007). Extended observations of volcanic SO_2 and sulfate aerosol in the stratosphere. *Atmospheric Chemistry and Physics Discussions*, *7*, 2857—2871.
Christie, D. M., Duncan, R. A., McBirney, A. R., Richards, M. A., White, W. M., Harpp, K. S., et al. (1992). Drowned islands downstream from the Galápagos hotspot imply extended speciation times. *Nature*, *355*, 246—248.
Crisp, J. (1995). *Volcanic SO2 alert – Version 3, EOS IDS Volcanology Team Data Product Document – Product #3288.*
Delmelle, P., Stix, J., Baxter, P., Garcia-Alvarez, J., & Barquero, J. (2002). Atmospheric dispersion, environmental effect and potential health hazard associated with the low-altitude gas plume of Masaya volcano, Nicaragua. *Bulletin of Volcanology*, *64*, 423—434.
Draxler, R. R., & Rolph, G. D. (2003). *HYSPLIT (HYbrid Single-Particle Lagrangian Integrated Trajectory) Model.*Silver Spring, MD: NOAA Air Rescources Laboratory accessed via NOAA ARL READY Website (http://www.arl.noaa.gov/ready/hysplit4.html)
Edmonds, M., Oppenheimer, C., Pyle, D. M., Herd, R. A., & Thompson, G. (2003). SO_2 emissions from Soufrière Hills Volcano and their relationship to conduit permeability, hydrothermal interaction and degassing regime. *Journal of Volcanology and Geothermal Research*, *124*(1-2), 23—43.
Geist, D. J., Harpp, K. S., Naumann, T. R., Poland, M., Chadwick, W. W., Hall, M., et al. (2008). The 2005 Eruption of Sierra Negra Volcano, Galápagos, Ecuador. *Bulletin of Volcanology*, *70*(6), 655—673.
Gillespie, A. R., Kahle, A. B., & Walker, R. E. (1986). Color Enhancement of highly correlated images. I. Decorrelation and HIS contrast stretches. *Remote Sensing of Environment*, *20*, 209—235.
GVN (2005). Sierra Negra. *Bulletin of the Global Volcanism Network*, *30*(09), 12—15.
Hall, M., Ramon, P., Tapia, W., & Caravajal, O. (2005). Caldera erupts starting 22nd October 2005 at fissure on caldera's inner N wall. *Bulletin of the Global Volcanism Network*, *30*, 09.
Henney, L.A., Watson, I.M., Realmuto, V.J., The use of ASTER to detect volcanic sulphur dioxide emissions from Fuego and Pacaya volcanoes, Guatemala, in review for: Remote Sensing of Environment.
Hoffman, D. J., Rosen, J. M., & Gringel, W. (1985). Delayed production of sulfuric acid condensation nuclei in the polar stratosphere from El Chichon volcanic vapors. *Journal of Geophysical Research*, *90*, 2341—2354.
Kearney, C., Watson, I. M., Bluth, G., Carn, S., Realmuto, V. J., A comparison of thermal infrared and ultraviolet space-based SO_2 retrievals at the 2003 Al-Mishraq State Sulfur plant fire. in review for: *Journal of Volcanology and Geothermal Research*.
Kerr, J. B., McElroy, C. T., & Olafson, R. A. (1980). Measurements of ozone with the Brewer ozone spectrophotometer. *Proceedings of the International Ozone Symposium*, *Vol. 1.* (pp. 74—79).
King, M. D., Kaufman, Y. J., Menzel, W. P., & Tanre, D. (1992). Remote sensing of cloud, aerosol, and water vapor properties from the moderate resolution imaging spectrometer (MODIS). *IEEE Transactions on Geoscience and Remote Sensing*, *30*(1), 2—27.
Krotkov, N. A., Krueger, A. J., & Bhartia, P. K. (1997). Ultraviolet optical model of volcanic clouds for remote sensing of ash and sulphur dioxide. *Journal of Geophysical Research*, *10*(D18), 21,891—21,904.
Krotkov, N. A., Yang, K., Carn, S. A., & Krueger, A. J. (2006). *EOS Aura Ozone Monitoring Instrument (OMI) OMSO2 README File.*: Goddard Space Flight Center (NASA) [Online]. Accessed on 09/11/07 from: http://avdc.gsfc.nasa.gov/Data/Aura/OMI/OMSO2/index.html
Krueger, A. J. (1983). Sighting of El Chichon sulfur dioxide with the Nimbus-7 total ozone mapping spectrometer. *Science*, *220*, 1377—1378 1983.
Krueger, A. J., Schaefer, S., Krotkov, N., Bluth, G., & Barker, S. (2000). Ultra-violet remote sensing of volcanic emissions and applications to aviation hazard mitigation. In P. J. Mouginis-Mark, J. A. Crisp, & J. H. Fink (Eds.), *Remote Sensing of Active Volcanism, Geophysical Monograph*, *Vol. 116*. (pp. 25—43). Washington, D.C., US: American Geophysical Union.
Krueger, A. J., Walter, L. S., Bhartia, P. K., Schnetzler, C. C., Krotkov, N. A., Sprod, I., et al. (1995). Volcanic sulfur dioxide measurements from the total ozone mapping spectrometer instruments. *Journal of Geophysical Research*, *100*(D7), 14,057—14,076.
Levelt, P. F., Hilsenrath, E., Leppelmeier, G. W., van den Oord, G. H. J., Bhartia, P. K., Tamminen, J., et al. (2006). Science objectives of the ozone monitoring instrument. *IEEE Transactions on Geoscience and Remote Sensing*, *44*(5), 1199—1208.
McPeters, R., Bhartia, P. K., Krueger, A., Herman, J., Wellemeyer, C., Seftor, C., et al. (1998). *Earth Probe Total Ozone Mapping Spectrometer (TOMS) Data Product User's Guide.* Greenbelt, Maryland: Goddard Space Flight Centre 20771 Technical Publication.
Munro, D. C., & Rowland, S. K. (1996). Caldera morphology in the western Galápagos and implications for volcano eruption behavior an mechanisms of caldera formation. *Journal of Volcanology and Geothermal Research*, *72*(1-2), 85—100.
Prata, A. J., Rose, W. I., Self, S., & O'Brien, D. M. (2003). Global, long-term sulphur dioxide measurements from the TOVS data: a new tool for studying explosive volcanism and climate. *Geophysical Monograph*, *139*, 75—92.
Prata, A.J., Watson, I.M., Rose, W.I., O'Brien, D.M., Realmuto, V., Bluth, G.J.S., et al. Volcanic sulfur dioxide concentrations derived from infrared satellite measurements. submitted for publication to: Geophysical Research Letters (Atmospheres).
Realmuto, V. J. (2001). In P. Mouginis-Mark, J. Crisp, & J. Fink (Eds.), *The potential use of earth observing system data to monitor the passive emission of sulphur dioxide from volcanoes. Remote sensing of active volcanism*, *Vol. 116*. (pp. 101—115): AGU Monograph.
Realmuto, V. J., Abrams, M. J., Buongiorno, M. F., & Pieri, D. C. (1994). The use of multispectral thermal infrared image data to estimate the sulfur dioxide flux from volcanoes: a case study from Mount Etna, Sicily, July 29, 1986. *Journal of Geophysical Research*, *99*(B1), 481—488.

Realmuto, V. J., Sutton, A. J., & Elias, T. (1997). Multispectral thermal infrared mapping of sulfur dioxide plumes: a case study from the East Rift Zone of Kilauea Volcano, Hawaii. *Journal of Geophysical Research*, *102*(B7), 15,057−15,072.

Realmuto, V. J., & Worden, H. M. (2000). Impact of atmospheric water vapor on the thermal infrared remote sensing of volcanic sulfur dioxide measurements: a case study from the Pu'u O'o vent of Kilauea Volcano, Hawaii. *Journal of Geophysical Research*, *105*, 21,497−21,508.

Robock, A. (2000). Volcanic eruptions and climate. *Reviews of Geophysics*, *38*(2), 191−219.

Robock, A., & Mao, J. (1995). The volcanic signal in surface temperature observations. *Journal of Climate*, *8*(5), 1086−1103.

Rose, W. I., Gu, Y., Watson, I. M., Yu, T., Bluth, G. J. S., Prata, A. J., et al. (2003). The February–March 2000 eruption of Hekla, Iceland from a satellite perspective. *Volcanism and the Earth's Atmosphere, Geophysical Monograph*, *139*, 107−132.

Salomonson, V. V., Barnes, W., Xiong, J., Kempler, S., & Masuoka, E. (2002). An overview of the earth observing system MODIS instrument and associated data systems performance. *Proceedings of the International Geoscience and Remote Sensing Symposium (IGARSS 02), Sydney, Australia*.

Schneider, D. J., Rose, W. I., Coke, L. R., & Bluth, G. J. S. (1999). Early evolution of a stratospheric volcanic eruption cloud as observed with TOMS and AVHRR. *Journal of Geophysical Research*, *104*(D4), 4037−4050.

Schoeberl, M. R., Douglass, A. R., Hilsenrath, E., Bhartia, P. K., Beer, R., William Waters, J., et al. (2006). Overview of the EOS Aura Mission. *IEE Transactions on Geoscience and Remote Sensing*, *55*(5), 1066−1074.

Sutton, A. J., Elias, T., Gerlach, T. M., & Stokes, J. B. (2001). Implications for eruptive processes by sulfur dioxide emissions from Kilauea Volcano, Hawaii, 1979–1997. *Journal of Volcanology and Geothermal Research*, *108*(1), 283−302 (20).

Thomas, W., Erbertseder, T., Ruppert, T., van Roozendael, M., Verdebout, J., Balis, D., et al. (2005). On the retrieval of volcanic sulfur dioxide emissions from GOME backscatter measurements. *Journal Atmospheric Chemistry*, *50*, 295−320.

Watson, I. M., Realmuto, V. J., Rose, W. I., Prata, A. J., Bluth, G. J. S., Gu, Y., et al. (2004). Thermal infrared remote sensing of volcanic emissions using the moderate resolution imaging spectroradiometer. *Journal of Volcanology and Geothermal Research*, *135*, 75−89.

Yang, K., Krotkov, N. A., Krueger, A. J., Carn, S. A., Bhartia, P. K., & Levelt, P. F. (2007). Retrieval of large volcanic SO_2 columns from the Aura Ozone Monitoring Instrument (OMI): comparisons and limitations. *Journal of Geophysical Research*, *112*, D24S43.